REFINING ESTIMATES OF THE SEISMIC VELOCITIES OF THE CRUST AND UPPER MANTLE

M.P. Barmin, N.M. Shapiro, and M.H. Ritzwoller

Center for Imaging the Earth's Interior, University of Colorado at Boulder
Campus Box 390, Boulder, CO, 80309-0390
E-mail: nshapiro@fignon.colorado.edu

V. Levin and J. Park

Department of Geology and Geophysics, Yale University
PO Box 208109, New Haven, CT 06520
E-mail: vadim@hess.geology.yale.edu

I. Summary

We discuss recent efforts to improve a global shear-velocity model of the crust and upper mantle by advancing surface wave methodology as well as by introducing new types of geophysical data in the inversion. The primary data-set used to construct the model consists of broad-band Rayleigh and Love wave group-velocity (CU-Boulder) and phase-velocity (Harvard, Utrecht) dispersion curves.

The first step of the inversion is surface wave tomography in which group and phase velocity maps are constructed. We present a new method of surface wave tomography called "diffraction tomography" that is based on a physical model of the surface wave Fresnel zone rather than on ray-theory and ad hoc regularization. Diffraction tomography accounts for path-length dependent sensitivity, wave-form healing and associated diffraction effects, and provides a more accurate assessment of spatially variable resolution than traditional tomographic methods.

The second step is Monte-Carlo inversion of the dispersion maps for an ensemble of acceptable shear velocity models of the crust and uppermost mantle. The result is a 3D seismic model with uncertainties that allows us to identify the key features worthy of interpretation; features that we call "persistent". The simultaneous inversion of broad-band fundamental mode group velocities with intermediate and long-period phase velocities greatly improves the vertical resolution of the 3-D model and the persistence of the estimated structures.

Because surface waves have limited vertical resolution, we apply constraints on the model derived from other types of geophysical observations. We consider two types of additional data: receiver functions and heat flow measurements (accompanying poster). Receivers functions are sensitive to sharp boundaries in and around the crust and, therefore, provide important constraints on crustal structure.

II. Surface wave diffraction tomography

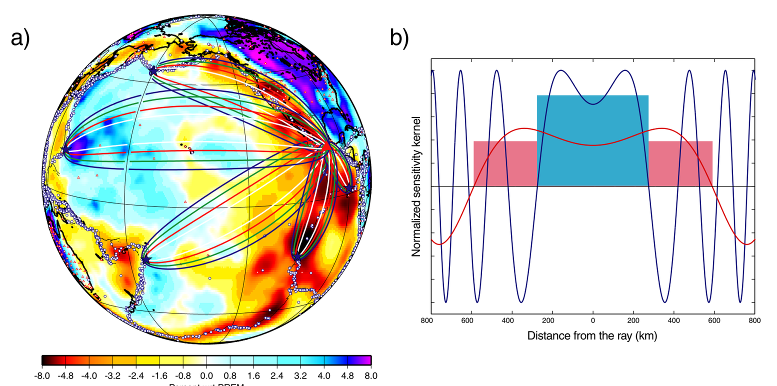

Figure 1. (a) First Fresnel zones plotted over the shear velocity model at 80 km depth for waves observed in Mexico (red triangle) originating from several epicentral regions (red star): Galapagos (2087 km), EPR (4493 km), Aleutians (7777 km), Tonga (8916 km), Marianas (11700). The Fresnel zones are for 20 s (white), 50 s (red), 100 s (green), and 150 s (blue) Rayleigh waves. Stations and events used in the group velocity data set are shown as small red triangles and blue circles, respectively.
(b) The transverse amplitude of the scattering sensitivity kernel at the center of the source-receiver path for 50 s Rayleigh wave phase velocity. The blue and red lines are the Born approximation kernels (Spetzler and Snieder, 2001) for epicentral distances of 2000 km and 8000 km, respectively. The blue and red shaded regions illustrate the crude box-car approximation to the scattering kernels we currently use in "diffraction tomography".

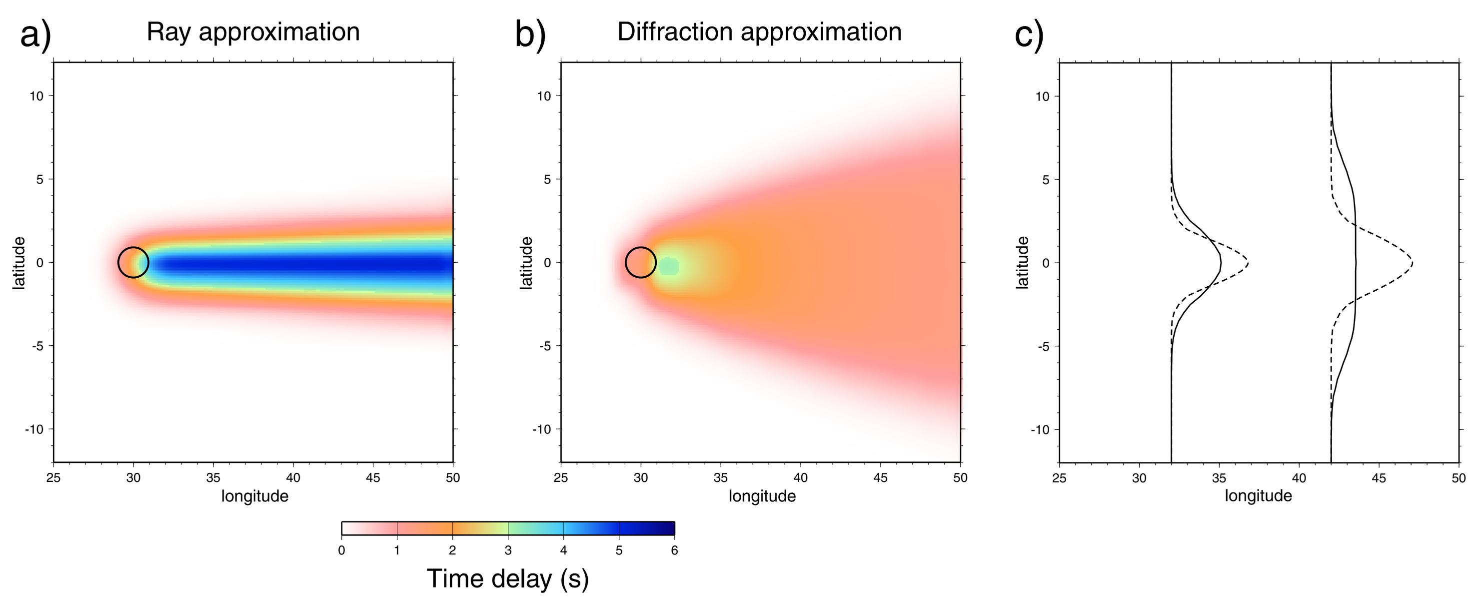

Figure 2. Demonstration of the effect of a small scatterer in (a) the ray-theoretic and (b) diffraction approximations. The scatterer is circular, with a Gaussian shaped profile with $\sigma = 1^o$ located 30^o (3333 km) from the source. In the ray approximation, the scatter casts a narrow travel time shadow whose amplitude does not reduce with distance. In the diffraction approximation, the shadow widens and the amplitude decays to model wavefront healing. (c) Profiles across the travel time shadow at 32^o and 43^o from the source (2^o and 13^o deg from the scatterer). The diffraction shadow (solid line) is flat due to the box-car shape of the scattering sensitivity kernel (Figure 1b). Diffraction lowers the amplitude of a travel time signal relative to ray theory (dashed line).

The surface wave dispersion maps (**Figure 3 and 4**) result from a surface wave tomographic method we call "diffraction tomography" that is based on a physical model of the surface wave Fresnel zone (**Figure 1**) rather than on ray-theory with ad-hoc smoothness constraints (e.g., Gaussian tomography, Barmin et al., 2001). Diffraction tomography accounts for path-length dependent sensitivity, wave-form healing and associated diffraction effects (**Figure 2**), and provides a more accurate assessment of spatially variable resolution than traditional tomographic methods (**Figures 6 and 7**). It is inspired by the pioneering efforts of Woodhouse and Girnius (1982), Wielandt (1987), Dahlen et al. (2000), Nolet and Dahlen (2000), Spetzler and Snieder (2001), and others. We find that:

1.Differences between diffraction and Gaussian tomography (ray theory with Gaussian smoothness constraints) are strongest at long periods, particularly in regions where the paths that sample the region are uniformly long; i.e., regions with poor stations and event coverage like the Pacific ocean.

2. Everything else being equal, diffraction tomography produces larger amplitudes than Gaussian tomography, particularly at long periods. This results largely from wavefront healing.

3. Resolution estimated with diffraction tomography differs strongly with estimates from Gaussian tomography, particularly at long periods in regions with poor station and event coverage. Resolution estimates derivating from diffraction tomography are spatially more variable and typically larger than those from Gaussian tomography. Largest differences exist in oceanic regions.

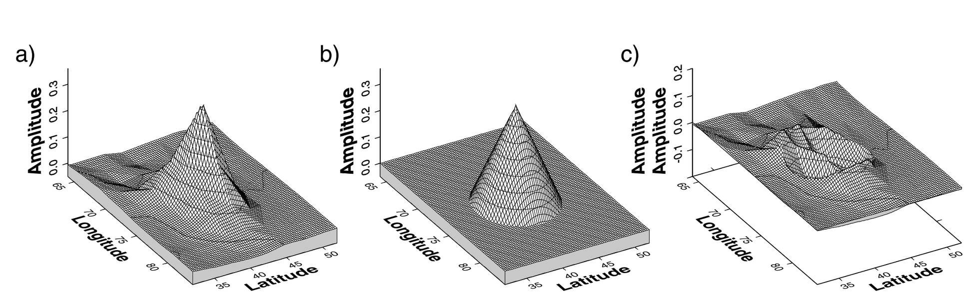

Figure 5. Resolution method. (a) For each grid point on the globe (2^ox2^o deg) we construct the resolution kernel, which is a row of the resolution matrix and can be presented as a map. (b) We fit a cone to the kernel, and identify the resolution with the full-width at the base of the cone. (c) Typically, a cone fits well, as shown by the difference between the resolution kernel and best-fitting cone. Perfect resolution would be a single non-zero point, implying a resolution of 444 km on a 2 deg x 2 deg grid.

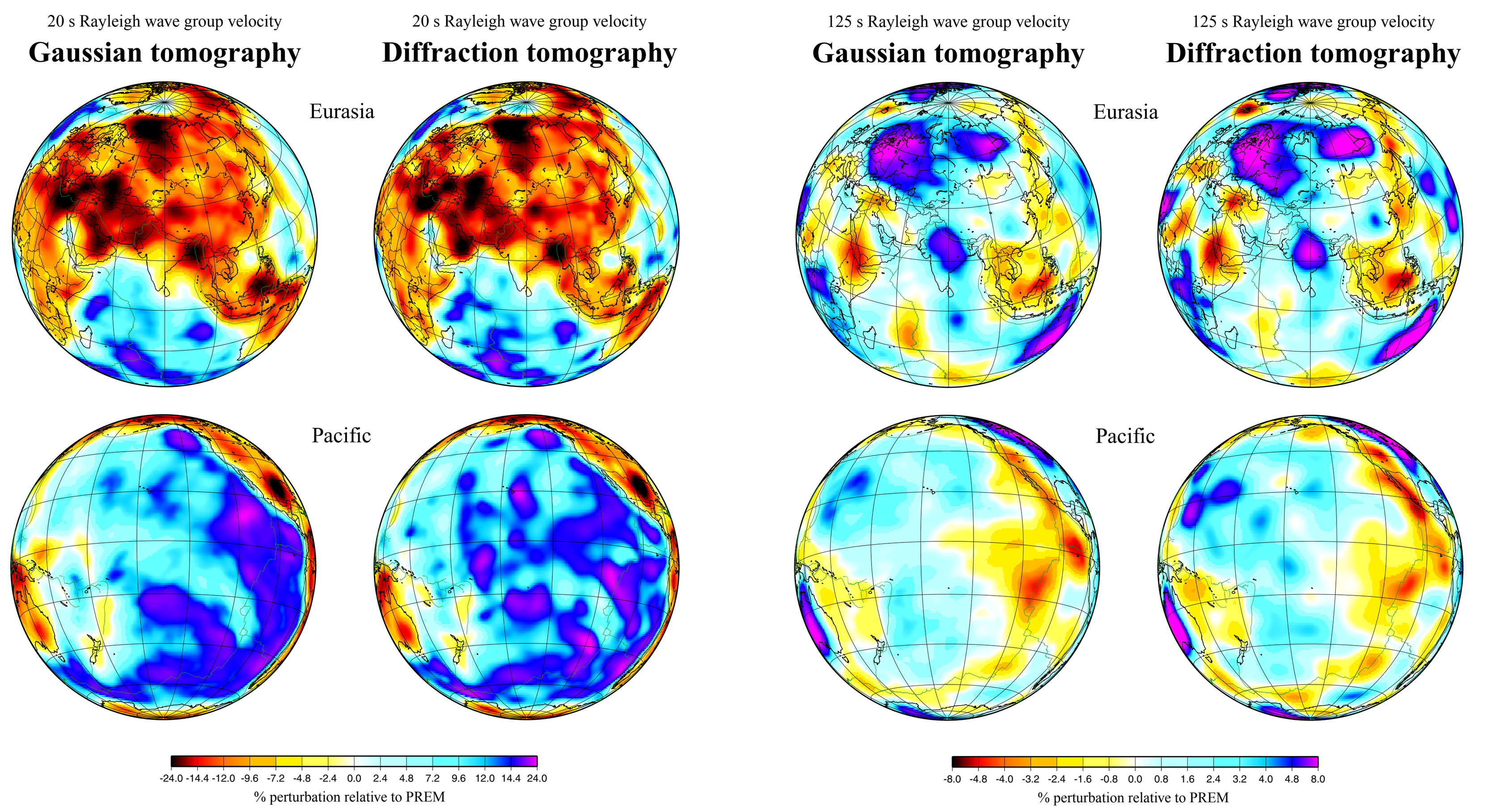

Figures 3 and 4. Results of diffraction tomography compared to tomography based on ray theory with Gaussian smoothness constraints (Gaussian tomography). Results here are for Rayleigh wave group velocities at 20 s and 125 s period. Diffraction and Gaussian tomography differ most at long periods in regions with poor station and event coverage (e.g., oceans). This is because Fresnel zones widen with period and taper near sources and receivers.

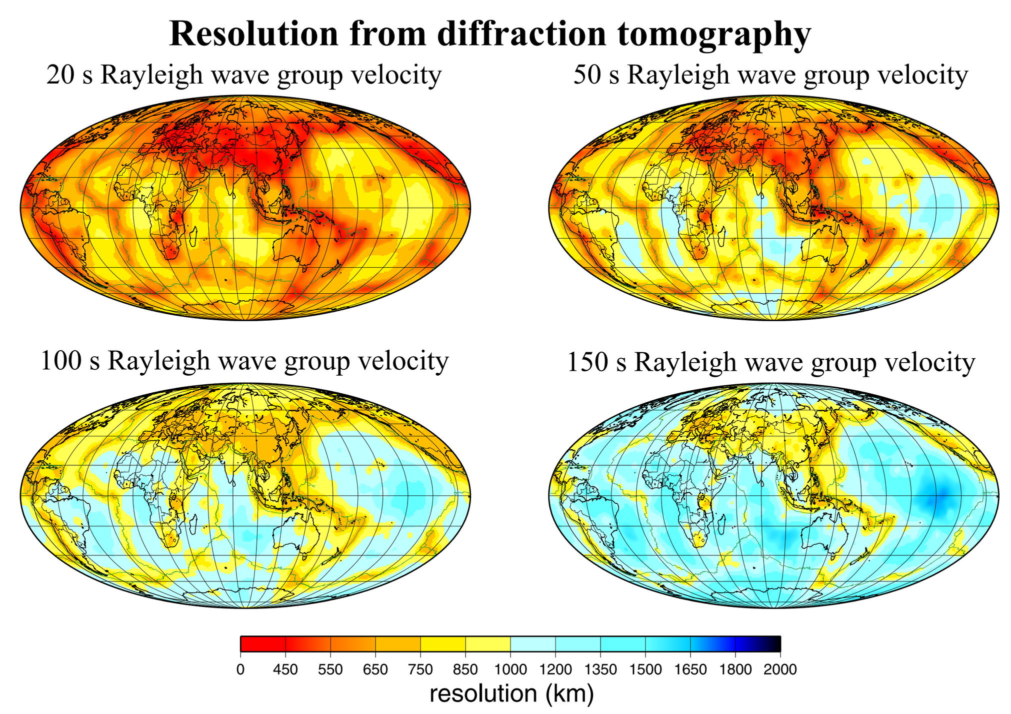

Figure 6. Resolution estimates for Rayleigh wave group velocity at 20, 50, 100, and 150 s using diffraction tomography

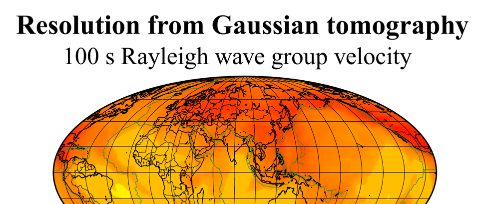

Figure 7. Resolution estimate for Rayleigh wave group velocity at 100 s using Gaussian tomography. The spatial uniformity of resolution is unrealistic, and results from the non-physical model of the surface wave sensitivity that does not account for path-length dependent width of the Fresnel zone.

III. Monte-Carlo Inversion

The shear velocity model is constructed on a 2^ox2^o grid globally to a depth of about 400 km using the method of Shapiro and Ritzwoller (2001). The goal of the procedure is to estimate the range of models that fit the dispersion maps subject to the uncertainties in the maps together with a priori information. The procedure culminates in a resampling of model space using a Monte Carlo method to produce a radially anisotropic V_S model. The ensemble of acceptable models is summarized with four numbers at each depth: the middle and the half-width of the corridor of acceptable models for both V_{sh} and V_{SV}. The half-width is an uncertainty estimate, designed to encompass both random and systematic errors. Results for two points are shown in **Figure 9**. The joint use of group and phase velocity data produces much better vertical resolution than either data set alone as shown in **Figure 10**.

The most robust features of the resulting model are those that appear in every member of the ensemble of acceptable model. We refer to these features as "persistent". Several vertical slices of the resulting 3D shear velocity model are shown in **Figure 11**, where the persistent features are identified with black contours.

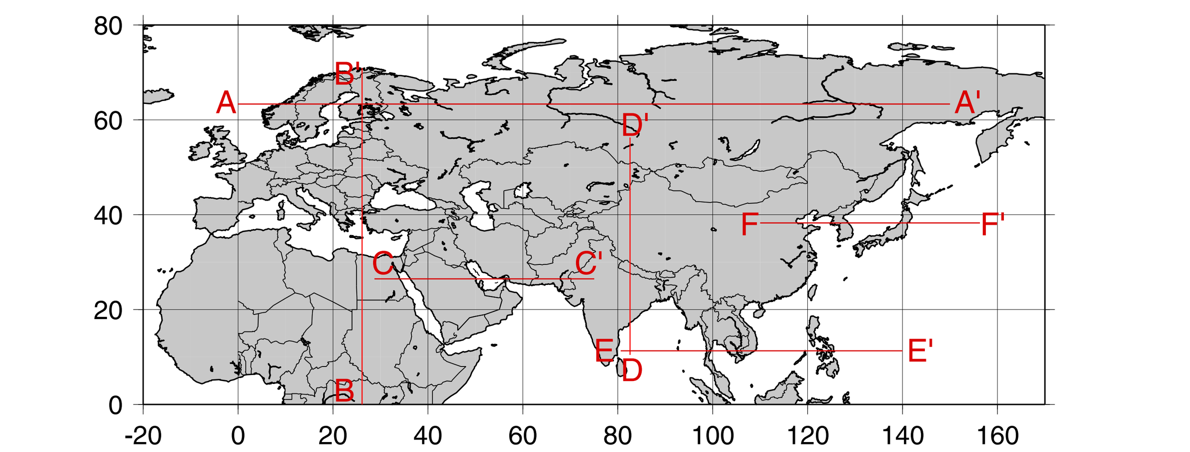

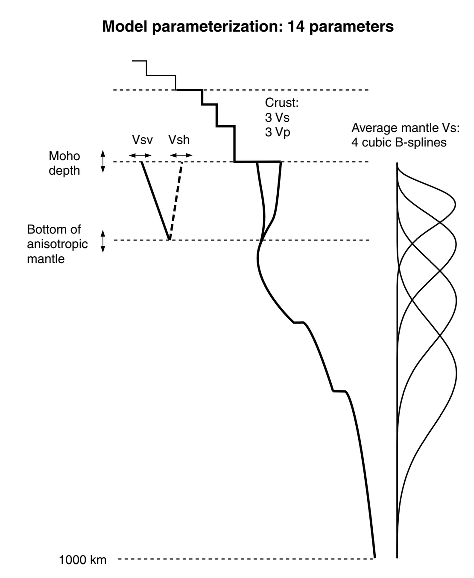

Figure 8. The parameterization of crustal and upper mantle structures. At each geographical point, the parameterization includes fourteen variables: a perturbation to sedimentary velocity, perturbations to both S and P velocities in each of three crustal layers, introduction of slopes in SV and SH velocities from Moho to a variable depth, and four cubic B-splines in the mantle.

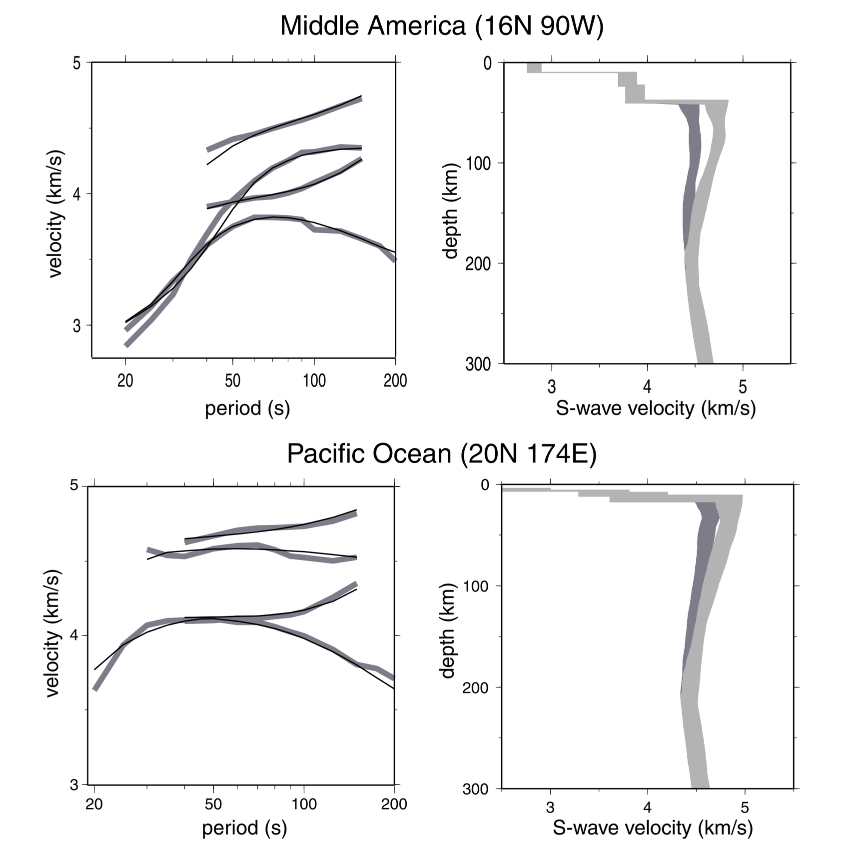

Figure 9. Data and Monte-Carlo inversion results shown for two points at: (TOP) Guatemala and (BOTTOM) the central Pacific. (LEFT COLUMN). Observed dispersion curves (thick grey lines, Rayleigh and Love wave group and phase velocity) and fit provided by the shear velocity model (black lines). (RIGHT COLUMN) The corridors indicate the ensemble of acceptable shear velocity models at each depth. The model is radially anisotropy between Moho and a depth of about 200 km: V_{SV} ne V_{sh}.

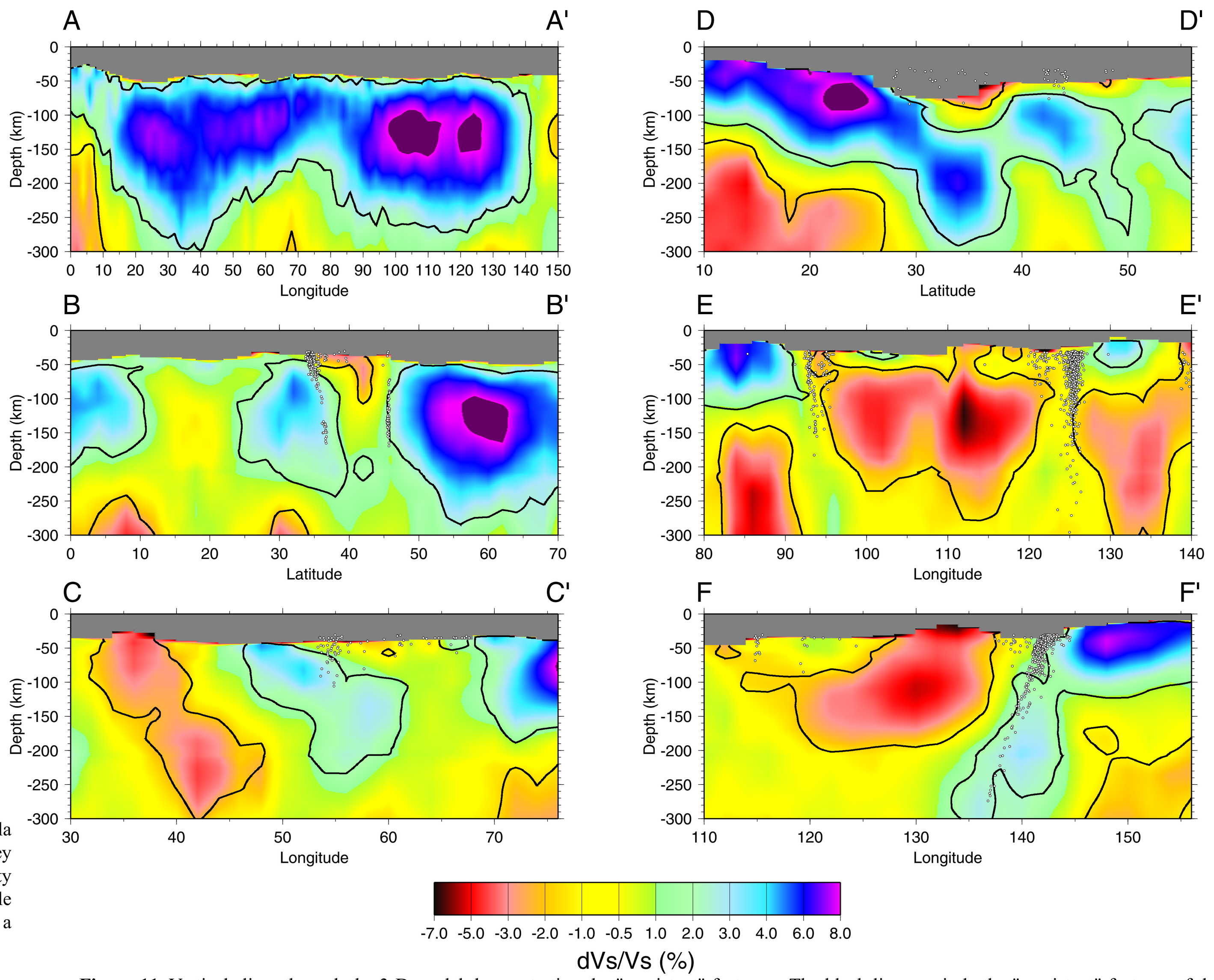

Figure 11. Vertical slices through the 3-D model demonstrating the "persistent" features. The black lines encircle the "persistent" features of the model; those features that appear in every member of the ensemble of acceptable models.

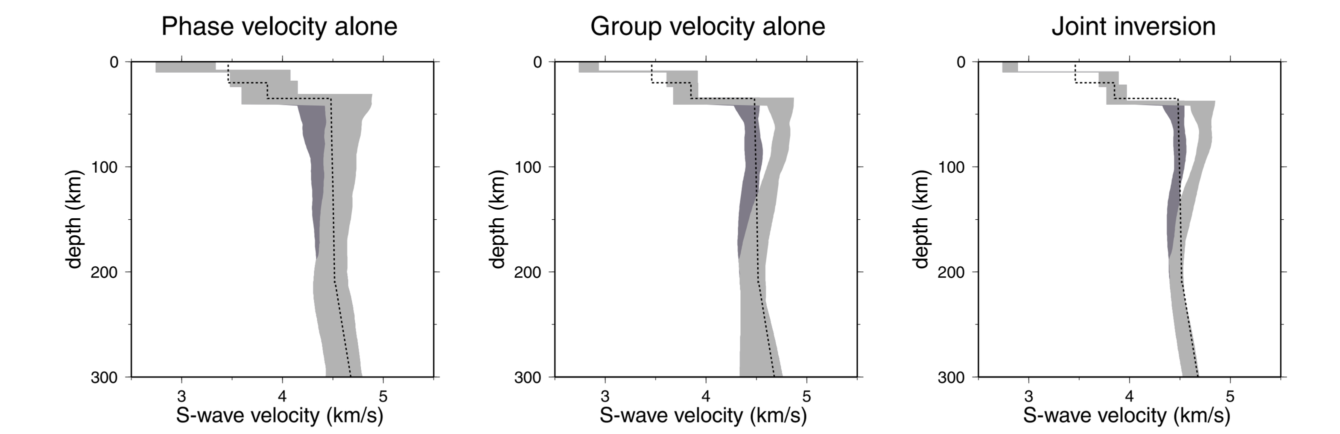

Figure 10. Example of how simultaneous use of group and phase velocity data improves vertical resolution. Here are plotted the ensembles of acceptable models using just phase velocity data (40 s - 150 s), just group velocity data (16 s - 150 s), or both simultaneously, for a point in Guatemala. The short period group velocities, sensitive exclusively to the crust, ameliorate the crust-mantle trade-off that afflicts phase velocity inversions, and long period phase velocities provide greater depth penetration than group velocities at the same periods. Thus, simultaneous inversion of both data sets provides much better vertical resolution than the use of either alone.

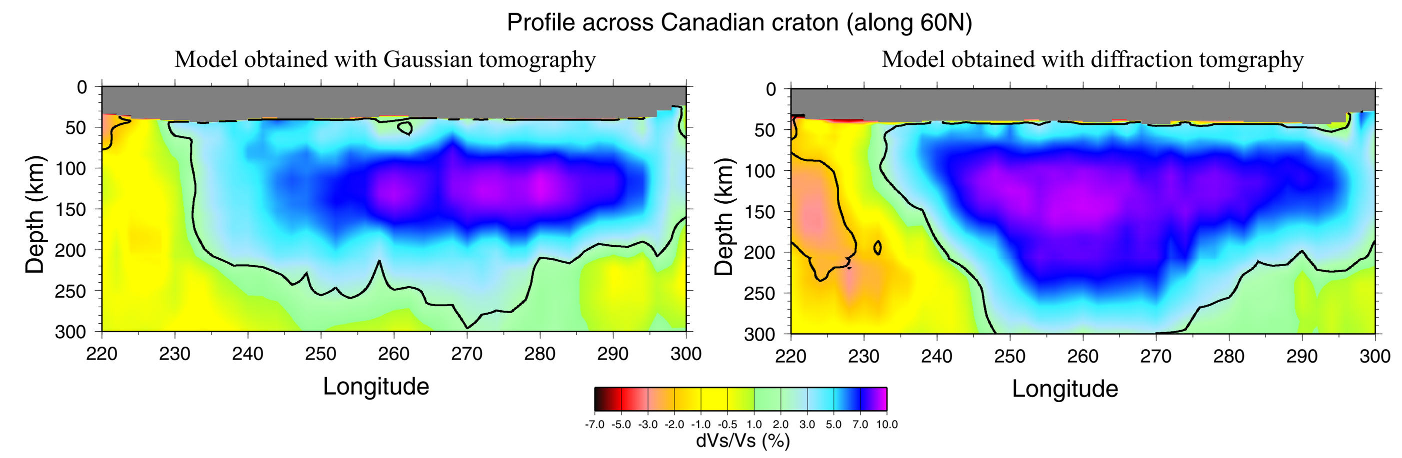

Figure 12. Example of the effect of diffraction tomography on the estimated model. These vertical slices are through the Canadian shield. Diffraction tomography tends to produce larger amplitudes at long periods than Gaussian tomography (e.g., Figure 4 for the 125 s Rayleigh wave in Eurasia). This means that some features, like continental cratons, will extend to greater depths in a 3D model derived from diffraction tomography, as shown here. As in **Figure 11**, the black lines surround persistent features of both models.

IV. Assimilating receiver functions in lithospheric inversion

Surface wave dispersion data alone cannot uniquely constrain crustal structures. The resulting uncertainties in crustal shear velocities are large and adversely affect the quality of the mantle part of the model. Tighter constraints on crustal structures are needed, to be used either as a priori information or applied simultaneously in the inversion. Receiver functions (RFs) provide one kind of useful information (e.g., Julia et al., 2000). A key challenge in combining surface wave dispersion and RFs is their different lateral resolutions. Ultimately, RFs may be most usefully merged with surface wave information when produced for an extended network or array, such as EarthScope.

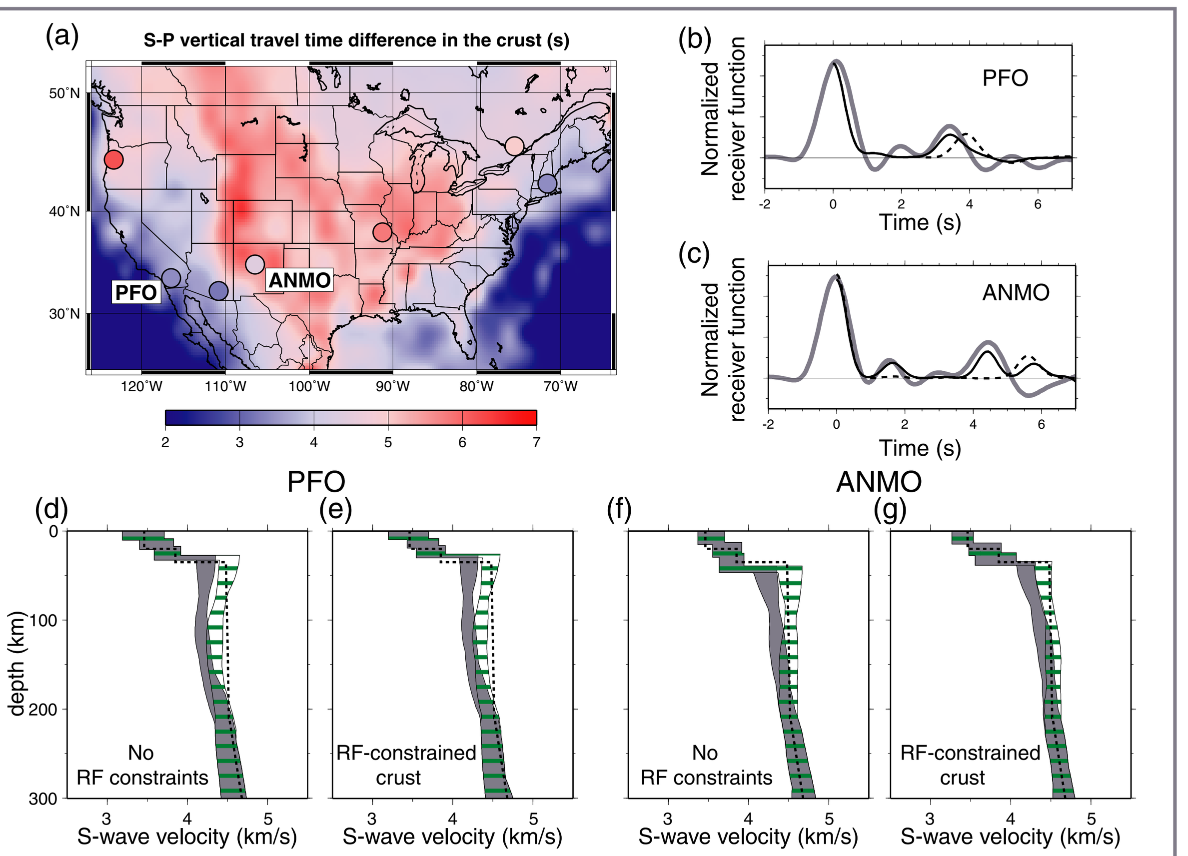

Figure 13. The effect of assimilating receiver functions (RF) in shear velocity inversions. (a) Maps of S-P vertical travel times in the crust predicted by our shear velocity model beneath the US. Colored circles show the S-P times estimated from RFs at several stations. (b) RF example for station PFO. Gray line is the observed RF, solid and dashed black lines are the RFs predicted from the shear velocity with and without the RF constraint, respectively. (c) Same as (b) at station ANMO. (d) Ensemble of models at station PFO obtained from the surface-wave inversion without RF constraints. Hatched regions are V_{sh}, grey-shaded regions are V_{SV}, and the dashed line is the 1D model ak135. (e) Similar to (d) but the crustal structure has been constrained by the observed RF. (f) and (g) Similar to (d) and (e), but for station ANMO. All RFs have been computed using the method of Park and Levin (2000).

References

Barmin, M.P., M.H. Ritzwoller, and A.L. Levshin, A fast and reliable method for surface wave tomography, *Pure appl. geophys.*, **158**, 1351-1375, 2001.

Dahlen, F.A., S.H. Hung, and G. Nolet, Frechet kernels for finite-frequency travel times: I. Theory, *Geophys. J. Int.*, **141**, 157-174, 2000.

Julia, J., C.J. Ammon, R.B. Herrmann, and A.M. Correig, Joint inversion of receiver function and surface wave dispersion observations, *Geophys. J. Int.*, **143**, 99-112, 2000.

Park, J. and V. Levin, Receiver functions from multiple-taper correlation estimates, *Bull. Seism. Soc. Am.*, **90**, 1507-1520, 2000.

Nolet, G. and F.A. Dahlen, Wave front healing and the evolution of seismic delay times, *J. Geophys. Res.*, **105**, 19,043-19,054, 2000.

Shapiro, N.M. and M.H. Ritzwoller, Monte Carlo inversion of broad band surface wave dispersion for a global shear velocity model of the crust and upper mantle, *Geophys. J. Int.*, submitted, 2001.

Spetzler, J. and R. Snieder, Are we exceeding the limits of the great circle approximation in global surface wave tomography? *Geoph. Res. Lett.*, **28**, 2341-2344, 2001.

Woodhouse, J.H. and T.P. Girnius, Surface waves and free oscillations in a regionalized earth model, *Geophys. J. R. Astr. Soc.*, **68**, 653-673, 1982.